

A forecast of using fast radio burst observations to constrain holographic dark energy

Xing-Wei Qiu,^a Ze-Wei Zhao,^a Ling-Feng Wang,^a Jing-Fei Zhang^a
and Xin Zhang^{a,b,c,1}

^aDepartment of Physics, College of Sciences, Northeastern University, Shenyang 110819, China

^bMOE Key Laboratory of Data Analytics and Optimization for Smart Industry, Northeastern University, Shenyang 110819, China

^cFrontiers Science Center for Industrial Intelligence and Systems Optimization, Northeastern University, Shenyang 110819, China

E-mail: qiuxingwei@stumail.neu.edu.cn, zhaozw@stumail.neu.edu.cn,
lingfengwang@stumail.neu.edu.cn, jfzhang@mail.neu.edu.cn,
zhangxin@mail.neu.edu.cn

Abstract. Recently, about five hundred fast radio bursts (FRBs) detected by CHIME/FRB Project have been reported. The vast amounts of data would make FRBs a promising low-redshift cosmological probe in the forthcoming years, and thus the issue of how many FRBs are needed for precise cosmological parameter estimation in different dark energy models should be detailedly investigated. Different from the usually considered $w(z)$ -parameterized models in the literature, in this work we investigate the holographic dark energy (HDE) model and the Ricci dark energy (RDE) model, which originate from the holographic principle of quantum gravity, using the simulated localized FRB data as a cosmological probe for the first time. We show that the Hubble constant H_0 can be constrained to about 2% precision in the HDE model with the Macquart relation of FRB by using 10000 accurately-localized FRBs combined with the current CMB data, which is similar to the precision of the SH0ES value. Using 10000 localized FRBs combined with the CMB data can achieve about 6% constraint on the dark-energy parameter c in the HDE model, which is tighter than the current BAO data combined with CMB. We also study the combination of the FRB data and another low-redshift cosmological probe, i.e. gravitational wave (GW) standard siren data, with the purpose of measuring cosmological parameters independent of CMB. Although the parameter degeneracies inherent in FRB and in GW are rather different, we find that more than 10000 FRBs are demanded to effectively improve the constraints in the holographic dark energy models.

¹Corresponding author.

Contents

1	Introduction	1
2	Methods and data	3
2.1	Brief description of the HDE and RDE models	3
2.2	Simulation of FRBs	5
2.3	Simulation of standard sirens	7
2.4	Cosmological data	10
3	Results and discussion	10
3.1	CMB+FRB	10
3.2	GW+FRB	14
3.3	Effect of DM_{host} uncertainty	15
4	Conclusion	16

1 Introduction

In 1998, two independent studies of distant supernovae discovered the accelerated expansion of the universe [1, 2], which is one of the most surprising astronomical discoveries in history. One can explain the accelerated expansion by introducing a component with negative pressure, usually called dark energy, and study its properties by cosmological observations. The cosmic microwave background (CMB) data measured by the *Planck* satellite [3] provided precise constraints on the cosmological parameters in the Λ cold dark matter (Λ CDM) model, which is usually regarded as the standard model of cosmology [4] with the origin of dark energy being explained as the cosmological constant Λ .

The Λ CDM model fits the current cosmological observations quite well, but it suffers from two theoretical puzzles: the fine-tuning problem and the coincidence problem [5]. Some dynamical dark energy models may relieve these problems [6–9]. However, the extra dark-energy parameters are hard to be precisely constrained by the CMB data alone due to the strong parameter degeneracies [10]. The baryon acoustic oscillation (BAO) measurements from galaxy redshift surveys [11–13] as a representative low-redshift cosmological probe are usually combined with the CMB data to break the cosmological parameter degeneracies. In the future, some other low-redshift cosmological probes are expected to yield large amounts of data, such as fast radio bursts (FRBs) and gravitational waves (GWs). Therefore, what precision to cosmological parameters these two non-optical probes could measure and how many events are needed for precise cosmological parameter estimation in different dark energy models are important questions at present.

FRBs are extremely bright, short-duration radio signals. One of the important characteristics of FRBs is the high dispersion measure (DM), which contains valuable information on the cosmological distance they have traveled. In 2007, the first FRB event, FRB010724, was observed by the 64-m Parkes Radio Telescope in Australia [14]. Although FRB010724 has a high Galactic latitude, it was previously thought to be caused by artificial interference due to its low signal-to-noise ratio (SNR). The second FRB event, FRB010621, was reported in ref. [15] in 2012. Later in 2013, Thornton et al. reported four new FRB samples [16],

which makes the study of FRBs become an important new direction in radio astronomy. Recently, the Canadian Hydrogen Intensity Mapping Experiment (CHIME)/FRB Project has released its first catalog of 535 FRBs, including 61 bursts from 18 previously reported repeating sources [17]. Till now, 19 FRBs’ host galaxies and cosmological redshifts have been identified [18–36]. These abundant data tremendously exceed the amount of current data of GWs with electromagnetic (EM) counterparts and further prove that FRBs may become a promising cosmological probe in the future.

The data of localized FRBs could be used to constrain cosmological parameters with the Macquart relation, which provide a relationship between DM_{IGM} and z [31]. There have been a series of works using FRBs as a cosmological probe to study the expansion history of the universe, such as estimating the cosmological parameters [37] and conducting cosmography [38] by using FRBs and Gamma-Ray Bursts association, using FRBs to measure Hubble parameter $H(z)$ [39] and the Hubble constant [40, 41], using the FRB data combined with the BAO data or the type Ia supernovae (SN) data to break the cosmological parameter degeneracies [42, 43], using FRBs to probe diffuse gas [44], using FRBs foreground mapping to constrain the cosmic baryon distribution [45], using FRBs to detect helium reionization [46], using FRB dispersion measures as distance measures [47], probing compact dark matter [48, 49], testing Einstein’s weak equivalence principle [50–52], and many other works [53–57]. For a recent review, see ref. [58].

In addition, there is also an idea of combining the FRB data with the GW data [59]. Wei et al. noticed the fact that DM is proportional to the Hubble constant H_0 while luminosity distance d_L is inversely proportional to H_0 , and they found that the product of DM from FRB and d_L from GW can yield a quantity free of H_0 , which may be useful in cosmological parameter estimation. Inspired by this work, ref. [60] introduced a cosmology-independent estimate of the fraction of baryon mass in the intergalactic medium (IGM). In ref. [61], the authors (including three of the authors in the present paper) also showed that combining the FRB data with the GW data could be helpful in cosmological parameter estimation. GWs provide a new method to measure the cosmic distance [62], dubbed as “standard sirens” [63], which successfully avoids the possible systematics in the cosmic distance ladder method. With the third-generation ground-based GW detectors, such as the Einstein Telescope (ET), large amounts of GW-EM events from the mergers of binary neutron stars (BNSs) are expected to be detected [64]. Thus, GWs may become a new precise cosmological probe to determine various cosmological parameters [64–71]. Especially, the GW data could be very helpful in breaking the cosmological parameter degeneracies when combined with other cosmological probes [72–77].

The capability of future FRB data in improving the cosmological parameter estimation in the w CDM and Chevallier-Polarski-Linder (CPL) models was studied in ref. [61]. It has been shown that the FRB data could break the parameter degeneracies in the CMB and GW data. But these two models and the most considered models in the literature [37–43] are parameterized and phenomenological models, and thus it is important to consider some dark energy models with deep and solid theoretical foundations and see whether the FRB data are still useful in cosmological parameter estimation in these dark-energy theoretical models. In this work, we investigate two dark energy models, i.e., the holographic dark energy (HDE) model and the Ricci dark energy (RDE) model. The HDE model is viewed to have a quantum gravity origin, which is constructed by combining the holographic principle of quantum gravity with the effective quantum field theory [78, 79]. Recently, a general covariant local field theory of HDE [80] and the structure formation in the effective field

theory of HDE is studied [81]. The HDE model not only can naturally explain the fine-tuning and coincidence problems [78], but also can fit the current and historical observational data well [82–91], and have the potential to solve some major cosmological problems, such as the Hubble tension [92]. The RDE model, as a theoretical variant of HDE, uses the average radius of the Ricci scalar curvature rather than the future event horizon of the universe as the infrared (IR) cutoff within the theoretical framework of HDE [93, 94]. Although the RDE model is not favored by the current observations [86], we still study it as a demonstration in the issue of forecasting the capability of FRB data in cosmological parameter estimation.

In this paper, we shall first combine the future FRB data with the current CMB data from *Planck*, and then we will study the combination of two future big-data low-redshift measurements, the FRB data and the GW standard siren data, in cosmological parameter estimation in the HDE and RDE models.

This paper is organized as follows. A brief description of the HDE and RDE models, the methods for simulating the FRB data and the GW data, and the current cosmological data are introduced in Section 2. The constraint results and relevant discussions are given in Section 3. We present our conclusions in Section 4. Throughout this paper, we adopt the units in which the speed of light equals 1.

2 Methods and data

2.1 Brief description of the HDE and RDE models

According to the Bekenstein entropy bound, an effective field theory considered in a box of size L with ultraviolet (UV) cutoff Λ_{uv} gives the total entropy $S = L^3 \Lambda_{\text{uv}}^3 \leq S_{\text{BH}} \equiv \pi M_{\text{Pl}}^2 L^2$, where S_{BH} is the entropy of a black hole with the same size L and $M_{\text{Pl}} = 1/\sqrt{8\pi G}$ is the reduced Planck mass. However, Cohen et al. pointed out that in quantum field theory a short distance (i.e., UV) cutoff is related to a long distance (i.e., IR) cutoff due to the limit set by forming a black hole, and proposed a more restrictive bound, i.e., the energy bound [95]. If the quantum zero-point energy density ρ_{vac} is relevant to a UV cutoff, the total energy of a system with size L would not exceed the mass of a black hole of the same size, namely, $L^3 \rho_{\text{vac}} \leq LM_{\text{Pl}}^2$. Obviously, the IR cutoff size of this effective quantum field theory is taken to be the largest length size compatible with this bound.

If we take the whole universe into account, the vacuum energy related to this holographic principle is viewed as dark energy, called “holographic dark energy”. The dark energy density can be expressed as [78]

$$\rho_{\text{de}} = 3c^2 M_{\text{Pl}}^2 L^{-2}, \quad (2.1)$$

where c is a dimensionless model parameter, which is used to characterize all the theoretical uncertainties in the effective quantum field theory, and this parameter is extremely important in phenomenologically determining the evolution of HDE.

If L is chosen to be the Hubble scale of the universe, then the dark energy density will be close to the observational result. However, Hsu pointed out that the equation of state (EoS) of dark energy in this case is not correct [96]. Li subsequently suggested that L should be chosen to be the size of the future event horizon [78],

$$R_{\text{eh}}(a) = a \int_t^\infty \frac{dt'}{a} = a \int_a^\infty \frac{da'}{H(a')a'^2}, \quad (2.2)$$

where a is the scale factor of the universe and $H(a)$ is the Hubble parameter as a function of a . In this case, the EoS of dark energy can realize the cosmic acceleration, and the model with such a setting is usually called the HDE model.

In the HDE model, the dynamical evolution of dark energy is governed by the following differential equations,

$$\frac{1}{E(z)} \frac{dE(z)}{dz} = -\frac{\Omega_{\text{de}}(z)}{1+z} \left(\frac{1}{2} + \frac{\sqrt{\Omega_{\text{de}}(z)}}{c} - \frac{3}{2\Omega_{\text{de}}(z)} \right), \quad (2.3)$$

$$\frac{d\Omega_{\text{de}}(z)}{dz} = -\frac{2\Omega_{\text{de}}(z)(1-\Omega_{\text{de}}(z))}{1+z} \left(\frac{1}{2} + \frac{\sqrt{\Omega_{\text{de}}(z)}}{c} \right), \quad (2.4)$$

where $E(z) \equiv H(z)/H_0$ is the dimensionless Hubble parameter and $\Omega_{\text{de}}(z)$ is the fractional density of dark energy. Solving these two differential equations with the initial conditions $\Omega_{\text{de}} = 1 - \Omega_{\text{m}0}$ and $E(0) = 1$ will obtain the evolutions of $\Omega_{\text{de}}(z)$ and $E(z)$. Then from the energy conservation equations,

$$\begin{aligned} \dot{\rho}_{\text{m}} + 3H\rho_{\text{m}} &= 0, \\ \dot{\rho}_{\text{de}} + 3H(1+w)\rho_{\text{de}} &= 0, \end{aligned} \quad (2.5)$$

where a dot represents the derivative with respect to the cosmic time t and ρ_{m} is the matter density, one can get the EoS of dark energy in the HDE model,

$$w = -\frac{1}{3} - \frac{2\sqrt{\Omega_{\text{de}}}}{3c}. \quad (2.6)$$

The RDE model is defined by choosing the average radius of the Ricci scalar curvature as the IR cutoff length scale in the theory. In FRW cosmology, the Ricci scalar takes

$$R = -6 \left(\dot{H} + 2H^2 + \frac{k}{a^2} \right), \quad (2.7)$$

where $k = 1, 0,$ and -1 stands for closed, flat, and open geometry, respectively, and we take $k = 0$ in the rest of this work. The dark energy density in the RDE model can be expressed as [93, 94]

$$\rho_{\text{de}} = 3\gamma M_{\text{pl}}^2 \left(\dot{H} + 2H^2 \right), \quad (2.8)$$

where γ is a positive constant redefined in terms of c . The evolution of the Hubble parameter is determined by the following differential equation,

$$E^2 = \Omega_{\text{m}} e^{-3x} + \gamma \left(\frac{1}{2} \frac{dE^2}{dx} + 2E^2 \right), \quad (2.9)$$

with $x \equiv \ln a$. The solution to this differential equation is found to be

$$E(z) = \left(\frac{2\Omega_{\text{m}}}{2-\gamma} (1+z)^3 + \left(1 - \frac{2\Omega_{\text{m}}}{2-\gamma} \right) (1+z)^{\left(4-\frac{2}{\gamma}\right)} \right)^{1/2}. \quad (2.10)$$

2.2 Simulation of FRBs

When EM waves propagate in plasma, they will interact with free electrons and generate dispersion. The group velocities of EM waves vary with respect to frequency, resulting in lower frequency signal being delayed. By measuring the time delay (Δt) of the pulse signal between the highest frequency (ν_h) and the lowest frequency (ν_l), we could obtain the dispersion measure of an FRB,

$$\text{DM} = \Delta t \frac{2\pi m_e}{e^2} \frac{(\nu_l \nu_h)^2}{\nu_h^2 - \nu_l^2}, \quad (2.11)$$

where m_e is the electron mass and e is the unit charge. The physical interpretation of DM is the integral of the electron number density along the line-of-sight, which is expressed as

$$\text{DM} = \int_0^D n_e(l) dl, \quad (2.12)$$

where n_e is the electron number density, l is the path length, and D is the distance to FRB. The DMs of current FRB observations are mainly in the range of $100 \sim 3000$ pc cm⁻³ [17], exceeding the amount of the dispersion contributed by the Milky Way by 10 to dozens of times.

Until now, the progenitors of FRBs have not been generally figured out (excluding a Galactic magnetar), so the real redshift distribution of FRBs is still an open issue. We assume that the comoving number density distribution of FRBs is proportional to the cosmic star formation history (SFH) [97, 98], and we thus obtain the SFH-based redshift distribution of FRBs [48],

$$N_{\text{SFH}}(z) = \mathcal{N}_{\text{SFH}} \frac{\dot{\rho}_* d_C^2(z)}{H(z)(1+z)} e^{-d_L^2(z)/[2d_L^2(z_{\text{cut}})]}, \quad (2.13)$$

where \mathcal{N}_{SFH} is a normalization factor, d_C is the comoving distance at redshift z , and $z_{\text{cut}} = 1$ is a Gaussian cutoff. The number of detected FRBs decreases at $z > z_{\text{cut}}$ due to the instrumental SNR threshold effect. The parameterized density evolution $\dot{\rho}_*(z)$ reads

$$\dot{\rho}_*(z) = l \frac{a + bz}{1 + (z/n)^d}, \quad (2.14)$$

with $l = 0.7$, $a = 0.0170$, $b = 0.13$, $n = 3.3$, and $d = 5.3$ [97, 99].

The total observed DM of an FRB consists of the contributions from the FRB's host galaxy, IGM, and the Milky Way [16, 37],

$$\text{DM}_{\text{obs}} = \text{DM}_{\text{host}} + \text{DM}_{\text{IGM}} + \text{DM}_{\text{MW}}. \quad (2.15)$$

The second term on the right hand side, DM_{IGM} , relates to cosmology, and its average value is expressed as

$$\langle \text{DM}_{\text{IGM}} \rangle = \frac{3H_0 \Omega_b f_{\text{IGM}}}{8\pi G m_p} \int_0^z \frac{\chi(z')(1+z') dz'}{E(z')}, \quad (2.16)$$

with

$$\chi(z) = Y_{\text{H}} \chi_{\text{e,H}}(z) + \frac{1}{2} Y_{\text{He}} \chi_{\text{e,He}}(z), \quad (2.17)$$

where $f_{\text{IGM}} = 0.83^1$ is the fraction of baryon mass in IGM [100], Ω_b is the present-day baryon fractional density, G is Newton's constant, m_p is the proton mass, $Y_{\text{H}} = 3/4$ is the hydrogen mass fraction, $Y_{\text{He}} = 1/4$ is the helium mass fraction, and the terms $\chi_{\text{e,H}}$ and $\chi_{\text{e,He}}$ are the ionization fractions for H and He, respectively. We take $\chi_{\text{e,H}} = \chi_{\text{e,He}} = 1$ [101], since both H and He are fully ionized when $z < 3$. In eqs. (2.16) and (2.17), the electron number density in IGM depends on two factors, i.e. the baryon number density in IGM and the free electron number fraction per baryon. The former factor is expressed by the product of the baryon number density of the whole universe, $\frac{3H_0^2\Omega_b}{8\pi Gm_p}$, and the proportion of baryons in IGM to the total baryons in the universe, f_{IGM} , and the latter factor is expressed by $\chi(z)$. Thus, the value of f_{IGM} is unrelated to $\chi(z)$ in which both H and He fully ionized are assumed.

From eq. (2.15), if we could determine DM_{obs} , DM_{host} , and DM_{MW} , the last remaining term DM_{IGM} could be measured. The total uncertainty of DM_{IGM} is expressed as

$$\sigma_{\text{DM}_{\text{IGM}}} = \left[\sigma_{\text{obs}}^2 + \sigma_{\text{MW}}^2 + \sigma_{\text{IGM}}^2 + \left(\frac{\sigma_{\text{host}}}{1+z} \right)^2 \right]^{1/2}. \quad (2.18)$$

We take the observational uncertainty $\sigma_{\text{obs}} = 1.5 \text{ pc cm}^{-3}$ [102]. From the Australia Telescope National Facility pulsar catalog [103], the average σ_{MW} is about 10 pc cm^{-3} for the sources at high Galactic latitudes ($|b| > 10^\circ$). We assume that the sources at high Galactic latitudes are included in the data, since the Galactic coordinates do not affect the predicted numbers of FRBs dramatically [104]. Due to the inhomogeneity of the baryon matter in IGM, the deviation of an individual event from the mean DM_{IGM} is described by σ_{IGM} . Here we use the following formula [60],

$$\sigma_{\text{IGM}} = \begin{cases} \frac{52-45z-263z^2+21z^3+582z^4}{1-4z+7z^2-7z^3+5z^4}, & z \leq 1.03, \\ -416 + 270z + 480z^2 + 23z^3 - 162z^4, & 1.03 < z \leq 1.13, \\ 38 \arctan[0.6z + 1] + 17, & z > 1.13, \end{cases} \quad (2.19)$$

which is fitted from the simulations in refs. [105, 106]. It should be noted that some assumptions in our work may be different from those in the numerical simulation, such as the value of baryon density. However, our fiducial values of cosmological parameters are consistent with those in ref. [60]. The reason of neglecting the details of numerical simulation is that for a forecast study, the error is more important than the fiducial value or the expectation value of $\text{DM}_{\text{IGM}}(z)$. The constraint precision of cosmological parameters directly depends on the error of $\text{DM}_{\text{IGM}}(z)$. Hence, although we make a simplification for convenience, using the fiducial values fully consistent with the numerical simulation [105, 106] would have negligible influence on the results. σ_{host} is hard to estimate because it depends on the individual properties of an FRB, for example, the type of the host galaxy, the location of FRB in the host galaxy, and the near-source plasma. We take $\sigma_{\text{host}} = 30 \text{ pc cm}^{-3}$ as the uncertainty of DM_{host} .

Now we discuss the observed event number of the FRB detection. The intrinsic event rate and luminosity distribution of FRBs [107–109], the sensitivity of a receiver, and the field of view of a telescope are important for the precise prediction on a certain experiment.

¹Figure 9 in ref. [100] shows the compilation of current observational measurements of the low-redshift baryon census. Baryons in collapsed form (galaxies, groups, and clusters), circumgalactic medium, intercluster medium, and cold neutral gas (H I and He I) make up about 17% of the total. Hence, 83% baryons of the universe should reside in the highly diffuse ionized gas in IGM.

However, in this work, we focus on the issue of how many localized FRBs are required to effectively constrain the cosmological parameters in the HDE and RDE models, regardless of any specific detectors. So, here we directly refer to the predictions in the literature. Recently, Lorimer pointed out that the ‘outrigger’ stations for CHIME/FRB will detect around 1000 sources over two years [110]. In the future, DSA-2000 would detect and localize FRBs at a rate of $\sim 10^3 - 10^4$ FRBs per year [111]; HIRAX could find dozens of localized FRBs per day [112]; ASKAP-CRAFT could localize 1500 FRBs with arcsecond accuracy over the next 5 years [58]. All these predictions support that the assumption of $\sim 10^3$ to 10^4 localized FRBs (with redshifts) for the observation of a few years is reasonable. Thus, we take $N_{\text{FRB}} = 1000$ as a normal expectation and $N_{\text{FRB}} = 10000$ as an optimistic expectation, with N_{FRB} being the event number of FRBs.

2.3 Simulation of standard sirens

To simulate the GW standard siren data generated by BNS mergers from ET, we first need to assume the redshift distribution of GWs [64, 70],

$$P(z) \propto \frac{4\pi d_C^2(z)R(z)}{H(z)(1+z)}, \quad (2.20)$$

where $R(z)$ is the time evolution of the burst rate with the form [70, 113, 114]

$$R(z) = \begin{cases} 1 + 2z, & z \leq 1, \\ \frac{3}{4}(5 - z), & 1 < z < 5, \\ 0, & z \geq 5. \end{cases} \quad (2.21)$$

By observing the GW waveform of a compact binary merger, one could independently determine the luminosity distance d_L to the GW source. If the redshift of the GW source is obtained through the observation of the EM counterpart, then the d_L - z relation can be established to study the expansion history of the universe [63].

An incoming GW signal $h(t)$ could be written as a linear combination of two wave polarizations in the transverse traceless gauge,

$$h(t) = F_+(\theta, \phi, \psi)h_+(t) + F_\times(\theta, \phi, \psi)h_\times(t), \quad (2.22)$$

where ψ is the polarization angle, (θ, ϕ) are the location angles of the GW source, and $+$ and \times denote the plus and cross polarizations, respectively. The antenna pattern functions of one Michelson-type interferometer of ET are [64]

$$F_+^{(1)}(\theta, \phi, \psi) = \frac{\sqrt{3}}{2} \left[\frac{1}{2}(1 + \cos^2\theta) \cos(2\phi) \cos(2\psi) - \cos\theta \sin(2\phi) \sin(2\psi) \right], \quad (2.23)$$

$$F_\times^{(1)}(\theta, \phi, \psi) = \frac{\sqrt{3}}{2} \left[\frac{1}{2}(1 + \cos^2\theta) \cos(2\phi) \sin(2\psi) + \cos\theta \sin(2\phi) \cos(2\psi) \right]. \quad (2.24)$$

Since the three interferometers of ET have inclined angles of 60° with each other, the other two pattern functions are $F_{+, \times}^{(2)}(\theta, \phi, \psi) = F_{+, \times}^{(1)}(\theta, \phi + 2\pi/3, \psi)$ and $F_{+, \times}^{(3)}(\theta, \phi, \psi) = F_{+, \times}^{(1)}(\theta, \phi + 4\pi/3, \psi)$.

Applying the stationary phase approximation to the time domain signal $h(t)$, we can get its Fourier transform $\tilde{h}(f)$ [64],

$$\tilde{h}(f) = \mathcal{A}f^{-7/6} \exp \left\{ i \left(2\pi f t_c - \pi/4 + 2\psi(f/2) - \varphi_{I,(2,0)} \right) \right\}, \quad (2.25)$$

where “ \sim ” above a function denotes the Fourier transform and \mathcal{A} is the amplitude in the Fourier space,

$$\mathcal{A} = \frac{1}{d_L} \sqrt{F_+^2(1 + \cos^2 \iota)^2 + 4F_\times^2 \cos^2 \iota} \sqrt{5\pi/96} \pi^{-7/6} \mathcal{M}_c^{5/6}, \quad (2.26)$$

where ι is the inclination angle between the direction of binary’s orbital angular momentum and the line of sight. The observed chirp mass is defined as $\mathcal{M}_c = (1 + z)M\eta^{3/5}$, with $M = m_1 + m_2$ being the total mass of coalescing binary system with component masses m_1 and m_2 , and $\eta = m_1 m_2 / M^2$ being the symmetric mass ratio. $\psi(f)$ and $\varphi_{I,(2,0)}$ are given by [115, 116]

$$\begin{aligned} \psi(f) &= -\psi_c + \frac{3}{256\eta} \sum_{i=0}^7 \psi_i (2\pi M f)^{(i-5)/3}, \\ \varphi_{I,(2,0)} &= \tan^{-1} \left(-\frac{2 \cos(\iota) F_\times}{(1 + \cos^2(\iota)) F_+} \right), \end{aligned} \quad (2.27)$$

where ψ_c is the coalescence phase, and the detailed expressions of the Post-Newtonian (PN) coefficients ψ_i are given in ref. [115]. Notice that here ψ ’s are the PN coefficients, different from the one in Eqs. (2.22)–(2.24), which is the polarization angle.

The total SNR of ET is

$$\rho = \sqrt{\sum_{i=1}^3 (\rho^{(i)})^2}, \quad (2.28)$$

where $\rho_i = \sqrt{\langle \tilde{h}^{(i)}, \tilde{h}^{(i)} \rangle}$, with the inner product being defined as

$$\langle a, b \rangle = 4 \int_{f_{\text{lower}}}^{f_{\text{upper}}} \frac{\tilde{a}(f) \tilde{b}^*(f) + \tilde{a}^*(f) \tilde{b}(f)}{2} \frac{df}{S_n(f)}, \quad (2.29)$$

$S_n(f)$ is the one-sided noise power spectral density. We use the interpolation method to fit the sensitivity data of ET to get the fitting function of $S_n(f)$ [117]. We choose $f_{\text{lower}} = 1$ Hz as the lower cutoff frequency and $f_{\text{upper}} = 2/(6^{3/2} 2\pi M_{\text{obs}})$ as the upper cutoff frequency with $M_{\text{obs}} = (m_1 + m_2)(1 + z)$ [64].

The luminosity distance d_L from GW observation is directly used to constrain cosmological parameters. The total error of d_L is expressed as

$$\sigma_{d_L} = \sqrt{\left(\sigma_{d_L}^{\text{inst}}\right)^2 + \left(\sigma_{d_L}^{\text{lens}}\right)^2 + \left(\sigma_{d_L}^{\text{PV}}\right)^2}, \quad (2.30)$$

where $\sigma_{d_L}^{\text{inst}}$, $\sigma_{d_L}^{\text{lens}}$, and $\sigma_{d_L}^{\text{PV}}$ are the instrumental error, the weak-lensing error, and the peculiar velocity error of luminosity distance, respectively. In our previous work [61], we adopted an approximation to the instrumental error, $\sigma_{d_L}^{\text{inst}} \simeq 2d_L/\rho$, in which the factor of 2 accounts for the maximal effect of the correlation between the luminosity distance and the inclination angle [118]. Indeed, this approximation does not exactly show the covariance between the luminosity distance and other parameters and may lead to biased results. Hence, in this work we employ a full Fisher matrix analysis to correctly account for the parameter correlations. The Fisher information matrix of the GW signal can be expressed as

$$\mathbf{F}_{ij} = \left\langle \frac{\partial \mathbf{h}(f)}{\partial \theta_i}, \frac{\partial \mathbf{h}(f)}{\partial \theta_j} \right\rangle, \quad (2.31)$$

where \mathbf{h} is given by three interferometers of ET,

$$\mathbf{h}(f) = \left[\tilde{h}_1(f), \tilde{h}_2(f), \tilde{h}_3(f) \right]^T, \quad (2.32)$$

and θ_i denotes the set of nine parameters $(\mathcal{M}_c, \eta, d_L, \theta, \phi, \psi, \iota, t_c, \psi_c)$ for a GW event. We then could estimate $\sigma_{d_L}^{\text{inst}}$ as

$$\sigma_{d_L}^{\text{inst}} = \Delta\theta_{d_L} = \sqrt{(F^{-1})_{d_L d_L}}, \quad (2.33)$$

where F_{ij} is the total Fisher information matrix for the ET with three interferometers.

The GW data used in this work are “bright sirens” and thus need the redshift information. The redshifts of GW sources are measured by their EM counterparts. In this work, we consider the short gamma ray bursts (SGRBs) and their afterglows as EM counterparts. Since SGRBs are supposed to be strongly beamed, we limit the observations of inclination angle from SGRBs within 20° . Therefore, in the Fisher matrix for each GW event, the sky location (θ, ϕ) , the inclination angle ι , the mass of each NS (m_1, m_2) , the coalescence phase ψ_c , and the polarization angle ψ are evenly sampled in the ranges of $[0, \pi]$, $[0, 2\pi]$, $[0, \pi/9]$, $[1, 2] M_\odot$, $[1, 2] M_\odot$, $[0, 2\pi]$, and $[0, 2\pi]$, respectively, where M_\odot is the solar mass. To eliminate the scatter of mock data, these parameters are randomly selected for 100 times to perform the Fisher matrix analysis, and we adopt the average results.

We then turn to the other two errors. The weak-lensing error is given by [119, 120]

$$\sigma_{d_L}^{\text{lens}}(z) = d_L(z) \times 0.066 \left[\frac{1 - (1+z)^{-0.25}}{0.25} \right]^{1.8}. \quad (2.34)$$

Here we introduce a delensing factor, i.e. the use of dedicated matter surveys along the line of sight of the GW event in order to estimate the lensing magnification distribution and thus remove part of the weak lensing uncertainty. Following refs. [121, 122], the delensing could be achieved 30% at $z = 2$ and the delensing factor can be expressed as

$$F_{\text{delens}}(z) = 1 - \frac{0.3}{\pi/2} \arctan(z/z_*), \quad (2.35)$$

with $z_* = 0.073$. The final lensing uncertainty on d_L is

$$\sigma_{d_L}^{\text{wl}}(z) = F_{\text{delens}}(z) \sigma_{d_L}^{\text{lens}}(z). \quad (2.36)$$

Here we use $\sigma_{d_L}^{\text{wl}}$ to replace $\sigma_{d_L}^{\text{lens}}$ in eq. (2.30).

The peculiar velocity of the source relative to the Hubble flow introduces an additional source of error. For the peculiar velocity error, we take the form in ref. [123]

$$\sigma_{d_L}^{\text{pv}}(z) = d_L(z) \times \left[1 + \frac{(1+z)^2}{H(z)d_L(z)} \right] \sqrt{\langle v^2 \rangle}, \quad (2.37)$$

where $H(z)$ is the Hubble parameter and $\sqrt{\langle v^2 \rangle}$ is the peculiar velocity of the GW source, set to be 500 km s^{-1} .

GW170817 was detected by the current second-generation ground-based GW detectors and its SGRB counterpart was detected by the *Neil Gehrels Swift* satellite [124]. In the future, with the higher sensitivity of the third-generation ground-based GW detectors and

the next-generation EM facilities, it is possible to detect much more GW events with redshift information. For example, ET is expected to detect about 10^5 BNS mergers per year but in which only $\sim 10^{-3}$ of the events with γ -ray bursts are toward us [125]. So, in the era of ET and CE, a few $\times 10^2$ GW events could be treated as “bright sirens” per year. Recently, Chen et al. conceived a future mission “*Swift* + +” and forecasted that about 910 GW bright siren events could be detected by CE and *Swift* + + with a 10-year observation [126]. In this work, we simulate 1000 standard siren events generated by BNS mergers within a 10-year observation of ET. In figure 1, we make a comparison between the FRB mock data in the normal expectation scenario and the GW mock data. We can see that in our simulations, the FRB data are mainly distributed below $z \approx 1.5$, but the GW data could extend to $z \approx 3$.

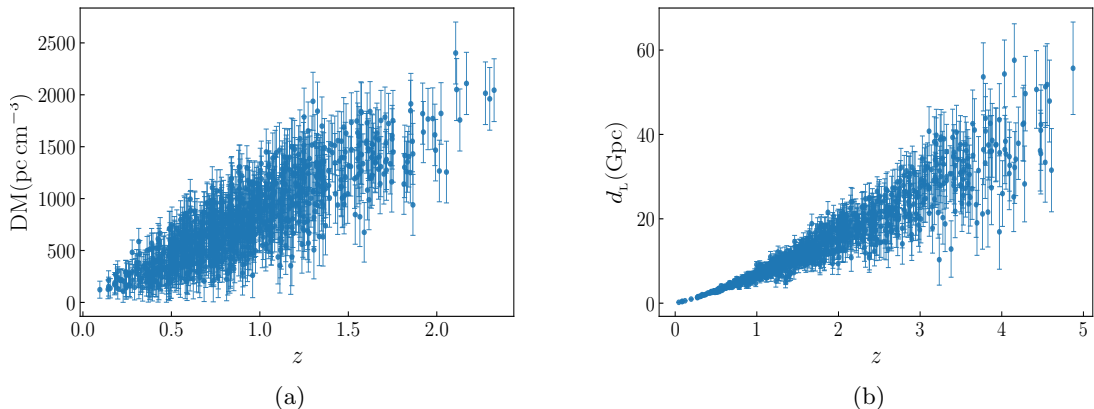


Figure 1. The mock FRB data (panel a) and the mock GW data from ET (panel b). The FRB data are simulated from the normal expectation scenario with 1000 FRB events, and the GW data are simulated from the 10-year observation of ET with 1000 BNS merger events.

2.4 Cosmological data

For the current mainstream cosmological data, we use the *Planck* CMB “distance priors” derived from the *Planck* 2018 data release [127], and the BAO measurements from 6dFGS at $z_{\text{eff}} = 0.106$ [11], SDSS-MGS at $z_{\text{eff}} = 0.15$ [12], and BOSS-DR12 at $z_{\text{eff}} = 0.38, 0.51, \text{ and } 0.61$ [13]. In the generation of the FRB and GW mock data, the fiducial values of cosmological parameters are taken to be the best-fit values of CMB+BAO+SN from ref. [128]. We use the Markov-chain Monte Carlo analysis [129] to obtain the posterior probability distribution of the cosmological parameters.

3 Results and discussion

3.1 CMB+FRB

In this subsection, we investigate the capability of the FRB data of breaking the parameter degeneracies inherent in the CMB data. We shall first discuss the improvement of the precision of cosmological parameters with the addition of the FRB data. Then we compare the capabilities of FRB and of BAO data in breaking the parameter degeneracies. The absolute errors (1σ) of the cosmological parameters in the HDE and RDE models are listed in

Model	Error	CMB	CMB+BAO	FRB1	CMB+FRB1	FRB2	CMB+FRB2
HDE	$\sigma(\Omega_m)$	0.032	0.012	0.062	0.022	0.026	0.012
	$\sigma(h)$	0.035	0.013	–	0.022	–	0.012
	$\sigma(c)$	0.18	0.087	0.55	0.11	0.44	0.057
	$10^2\sigma(\Omega_b h^2)$	0.015	0.015	0.56	0.014	0.53	0.0097
RDE	$\sigma(\Omega_m)$	0.060	–	0.087	0.043	0.032	0.020
	$\sigma(h)$	0.057	–	–	0.045	–	0.021
	$\sigma(\gamma)$	0.019	–	0.24	0.014	0.058	0.0081
	$10^2\sigma(\Omega_b h^2)$	0.015	–	0.67	0.013	0.51	0.0076

Table 1. Absolute errors (1σ) of the cosmological parameters in the HDE and RDE models by using the CMB, CMB+BAO, FRB1, CMB+FRB1, FRB2, and CMB+FRB2 data. FRB1 and FRB2 denote the FRB data in the normal expectation scenario (i.e., $N_{\text{FRB}} = 1000$) and optimistic expectation scenario (i.e., $N_{\text{FRB}} = 10000$), respectively.

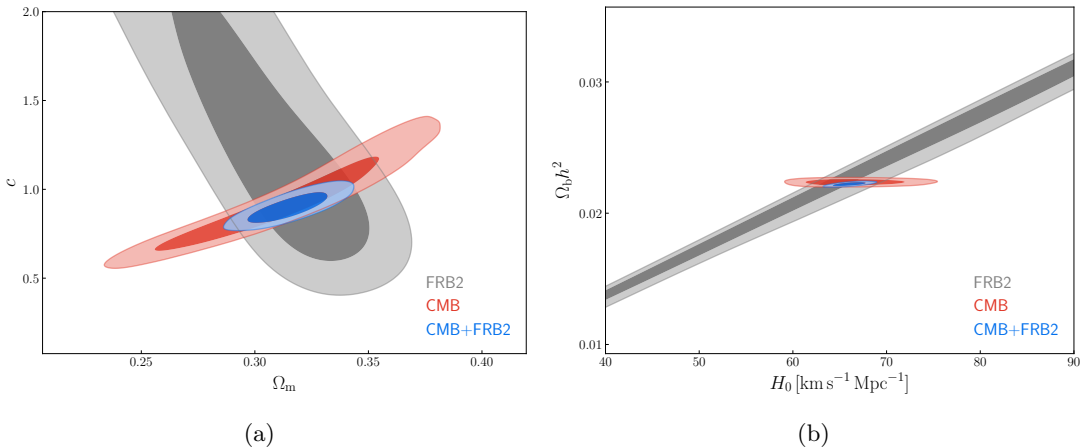


Figure 2. Two-dimensional marginalized contours (68.3% and 95.4% confidence levels) in the Ω_m - c plane (panel a) and the H_0 - $\Omega_b h^2$ plane (panel b) for the HDE model, by using the FRB, CMB, and CMB+FRB data. Here, the FRB data are simulated based on the optimistic expectation scenario.

table 1. We use FRB1 and FRB2 to denote the FRB data in the normal expectation (i.e., $N_{\text{FRB}} = 1000$) and the optimistic expectation (i.e., $N_{\text{FRB}} = 10000$), respectively. Here, for a cosmological parameter ξ , we use $\sigma(\xi)$ to denote its absolute error, and we also use the relative error $\varepsilon(\xi) = \sigma(\xi)/\xi$ in the following discussions.

From table 1 we see that the cosmological constraints from the FRB1 and FRB2 data are looser than those from the CMB data (except for Ω_m from FRB2). However, with combining the CMB and FRB data, the constraints from the CMB+FRB1 and CMB+FRB2 data are both evidently improved compared with those from the CMB data alone. As shown in figure 2, in the HDE model, Ω_m and c are positively correlated in the CMB data, but they are anti-correlated in the FRB data. Combining the CMB and FRB data breaks the

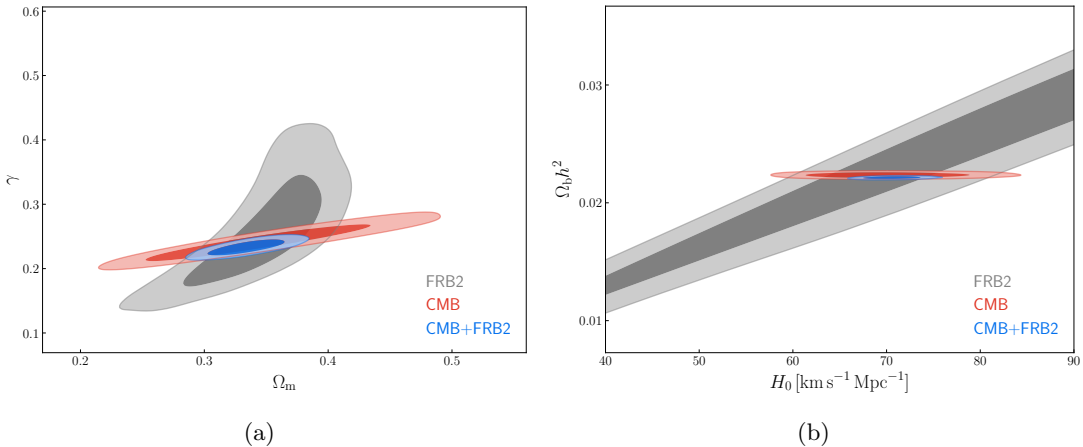


Figure 3. Two-dimensional marginalized contours (68.3% and 95.4% confidence levels) in the Ω_m - γ plane (panel a) and the H_0 - $\Omega_b h^2$ plane (panel b) for the RDE model, by using the FRB, CMB, and CMB+FRB data. Here, the FRB data are simulated based on the optimistic expectation scenario.

parameter degeneracies, and thus improves the constraints on the EoS parameters of dark energy and the matter density parameter. For the HDE model, the CMB data combined with the FRB1 and FRB2 data give the results $\varepsilon(c) = 11.7\%$ and $\varepsilon(c) = 6.3\%$, respectively. The absolute errors of c are reduced by about 40.0% and 67.7% by combining the FRB1 and FRB2 data with the CMB data, respectively. It is worth emphasizing that the constraint $\varepsilon(c) = 6.3\%$ is close to the constraint precision given by the CMB+BAO+SN data [128]. That is to say, using only the future FRB data combined with the CMB data could provide precise cosmological constraints comparable with the current mainstream data. For the RDE model, it is shown in figure 3 that the FRB data also break the parameter degeneracies inherent in the CMB data. The CMB data combined with the FRB1 and FRB2 data give $\varepsilon(\gamma) = 5.9\%$ and $\varepsilon(\gamma) = 3.5\%$, respectively. The absolute errors of γ are reduced by about 24.3% and 56.2%, by adding the FRB1 and FRB2 data to the CMB data, respectively.

Then we turn our attention to the constraints on the baryon density Ω_b and the Hubble constant H_0 . Using big bang nucleosynthesis (BBN) and CMB can precisely determine the value of $\Omega_b h^2$, however, in the nearby universe, the observed baryons in stars, the cold interstellar medium, residual Ly α forest gas, O VI, broad H I Ly α absorbers, and hot gas in clusters of galaxies account for only $\sim 50\%$ of the baryons [58, 130]. This is called the missing baryon problem. On the other hand, for the measurements of the Hubble constant, in recent years there appeared the puzzle of ‘‘Hubble tension’’. The values of the Hubble constant derived from different observations show strong tension, which actually reflects the inconsistency of measurements between the early universe and the late universe [131–141]. One may expect to precisely measure $\Omega_b h^2$ and H_0 with powerful low-redshift probes.

In figure 2(b), we show the marginalized posterior probability distribution contours in the H_0 - $\Omega_b h^2$ plane for the HDE model. We see that H_0 and $\Omega_b h^2$ are strong positively correlated when using the FRB data alone, because DM_{IGM} is proportional to $H_0 \Omega_b$ [see eq. (2.16)]. It is found that solely using the FRB2 data cannot constrain H_0 , but can effectively constrain $\Omega_b h^2$, giving the result of $\sigma(\Omega_b h^2) \approx 0.005$, which is an about 22.7% constraint. Although the precision is still low, the method of using the FRB observation has been proven to provide a potential way to solve the missing baryon problem. The CMB data can place tight constraint

on $\Omega_b h^2$, and thus the data combination FRB+CMB can give a precise measurement on H_0 . For the HDE model, the simulated FRB1 data combined with the current CMB data could give the result $\varepsilon(h) = 3.3\%$, which is reduced by 37.1% compared to using the CMB data alone. The data combination CMB+FRB2 can give the result $\varepsilon(h) = 1.8\%$, which roughly equals the measurement precision of the SH0ES value [142]. For CMB+FRB2 in the RDE model, the FRB2 data combined with the CMB data could give $\varepsilon(h) = 2.9\%$, and the error of h are reduced by about 64% by adding the FRB2 data to the CMB data.

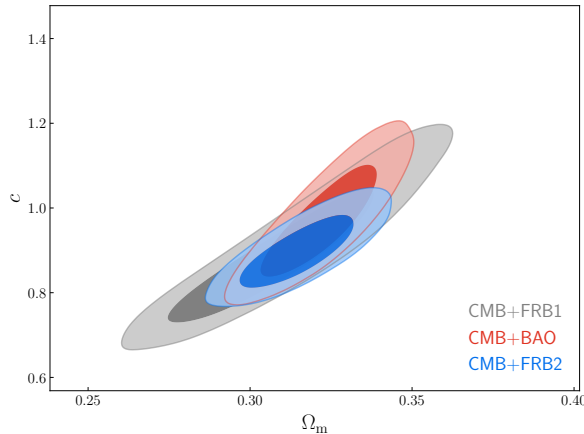


Figure 4. Two-dimensional marginalized contours (68.3% and 95.4% confidence levels) in the Ω_m - c plane for the HDE model, by using the CMB+FRB1, CMB+BAO, and CMB+FRB2 data.

Moreover, we also compare the capabilities of the CMB+FRB and CMB+BAO data of constraining cosmological parameters. From figure 4 we can see that the constraints from the CMB+FRB2 data are comparable to those from the CMB+BAO data, even slightly better. In the HDE model, both the CMB+FRB2 and CMB+BAO data give a constraint of $\sigma(\Omega_m) = 0.012$. For the parameter c , the CMB+FRB2 and CMB+BAO data give the results $\sigma(c) = 0.056$ and $\sigma(c) = 0.087$, respectively. It indicates that the FRB2 data have similar capability of breaking parameter degeneracies as the BAO data.

Finally, we explain why combining the CMB and FRB data can break the parameter degeneracies. The correlation between parameters c and Ω_m is related to the used observational data. Different data measure different physical quantities, thus leading to different correlations between parameters. For the FRB data, we can plot $\langle \text{DM}_{\text{IGM}} \rangle$ as a function of c (Ω_m) while all the other parameters are fixed, as shown in the left (right) panel of Fig. 5. The results are calculated at the mean value of our mock FRB data's redshift, $z = 1$, as a representative. We find that the parameters c and Ω_m are both inversely proportional to $\langle \text{DM}_{\text{IGM}} \rangle$. Therefore, c and Ω_m are anti-correlated when using the FRB data to constrain them, since $\langle \text{DM}_{\text{IGM}} \rangle$ is the effective observational quantity and should be approximately viewed as a fixed value at a specific redshift.

The correlation between parameters c and Ω_m in the CMB data can also be evaluated in the above method. Here we directly refer to Fig. 3 in ref. [85] to show that c and Ω_m are positively correlated when they are constrained by CMB data. The different correlations between c and Ω_m in the FRB and CMB data thus lead to the parameter degeneracies being broken.

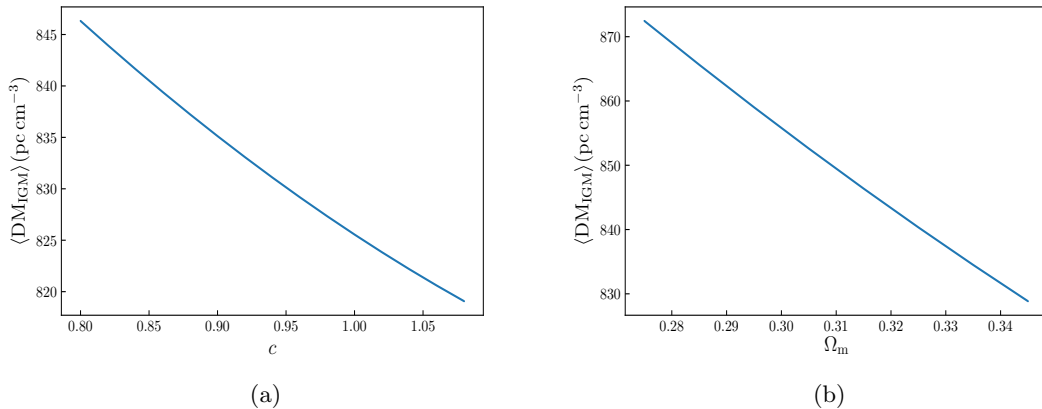


Figure 5. $\langle DM_{IGM} \rangle$ as a function of c (panel a) and Ω_m (panel b) calculated at $z = 1$. Other cosmological parameters are fixed to the fiducial values.

3.2 GW+FRB

	Error	GW	GW+FRB	CMB+GW	CMB+GW+FRB
HDE	$\sigma(\Omega_m)$	0.024	0.016	0.0059	0.0052
	$\sigma(h)$	0.010	0.0095	0.0064	0.0054
	$\sigma(c)$	0.21	0.16	0.045	0.035
	$10^2\sigma(\Omega_b h^2)$	–	0.011	0.015	0.0074
RDE	$\sigma(\Omega_m)$	0.012	0.011	0.0090	0.0082
	$\sigma(h)$	0.015	0.014	0.0093	0.0086
	$\sigma(\gamma)$	0.028	0.020	0.0067	0.0059
	$10^2\sigma(\Omega_b h^2)$	–	0.011	0.014	0.0069

Table 2. Absolute errors (1σ) of the cosmological parameters in the HDE and RDE models by using the GW, GW+FRB, CMB+GW, and CMB+GW+FRB data. Here, the FRB data are simulated based on the optimistic expectation scenario.

In addition to the FRB observation, the GW observation is another powerful cosmological probe. As demonstrated in ref. [61], the FRB and GW observation could help each other to break the parameter degeneracies in the w CDM and CPL models. In this subsection, we further study these two cosmological probes in the HDE and RDE models, and the FRB data are simulated based on the optimistic expectation scenario.

From table 2, we see that the constraints from the data combination GW+FRB are slightly improved compared with the GW data alone. But from figure 6 we find that the parameter degeneracy orientations formed by GW and by FRB are nearly orthogonal. The inclusion of the FRB data reduces the relative error on Ω_m from 8.4% to 5.2% in the HDE model. The constraints on Ω_m and $\Omega_b h^2$ from the GW+FRB data are comparable to those

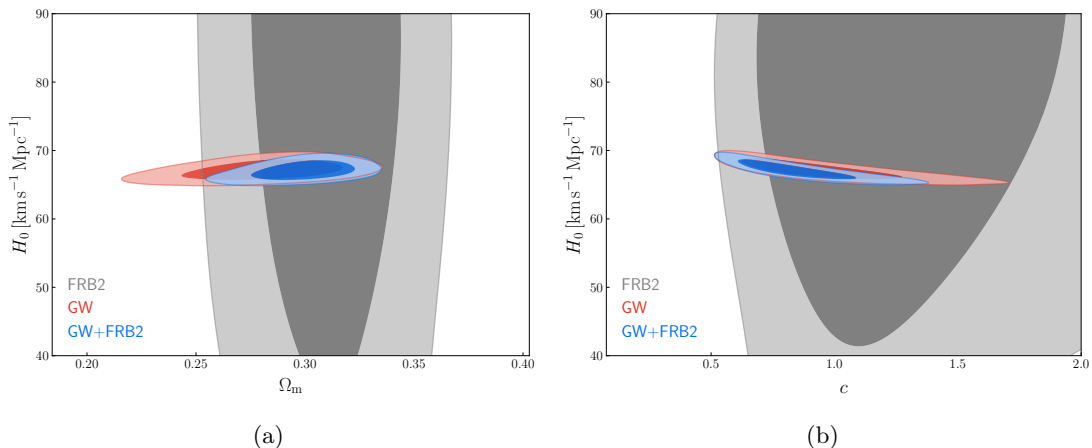


Figure 6. Two-dimensional marginalized contours (68.3% and 95.4% confidence levels) in the Ω_m – H_0 plane (panel a) and the c – H_0 plane (panel b) for the HDE model, by using the FRB, GW, and GW+FRB data. Here, the FRB data are simulated based on the optimistic expectation scenario.

from the CMB+BAO data. However, neither the GW data nor the FRB data can give tight constraints on the parameter c . The data combination GW+FRB gives $\varepsilon(c) = 18.0\%$, which is only slightly better than the constraint with CMB alone. For the Hubble constant H_0 , the FRB data actually contribute a little to the joint constraint of GW+FRB, since the GW data alone are able to precisely constrain H_0 but FRB alone cannot constrain it. Compared with the results in the w CDM model [61], the improvement of parameter constraint by adding 10000 FRB data into the GW data is weaker in the HDE model. For example, the improvements of the constraints on Ω_m are 53% and 33% in the w CDM and HDE models, respectively. Therefore, we find that, for constraining the HDE model, much more FRB data are needed to be combined with the GW data.

The results from the data combination CMB+GW+FRB further confirm this statement. The inclusion of the FRB data in the data combination CMB+GW+FRB tinily improves the constraints on Ω_m and H_0 , and the contributions to the constraints mainly come from CMB+GW. Nevertheless, the CMB+GW data can only constrain c to the precision of around 5%, which is still far away from the standard of precision cosmology. Compared to the GW data, the FRB data are more likely to be enlarged to a larger sample. Furthermore, the event rate of FRBs detected by SKA could be at least 2–3 orders of magnitude larger than the sample size we have considered [104]. With the accumulation of more abundant and precise data, FRBs would provide a tight constraint on the EoS of dark energy, so we expect that in the future the large amounts of FRBs observed by SKA may have the potential to help the joint constraint on c achieve the precision around 1%.

3.3 Effect of DM_{host} uncertainty

In the above analyses, we have assumed that the DM_{host} uncertainty is 30 pc cm^{-3} . The progenitors of FRBs are actually not clear and some factors are still open issues. The treatment of $\sigma_{\text{host}} = 30 \text{ pc cm}^{-3}$ thus could be regarded as an optimistic scenario. In this subsection, we perform an analysis based on a more conservative scenario with $\sigma_{\text{host}} = 150 \text{ pc cm}^{-3}$. The FRB data of this conservative scenario is represented by FRB3. The constraint results of cosmological parameters are shown in table 3.

Model	Error	FRB3	CMB+FRB3
HDE	$\sigma(\Omega_m)$	0.025	0.013
	$\sigma(h)$	–	0.013
	$\sigma(c)$	0.44	0.058
	$10^2\sigma(\Omega_b h^2)$	0.51	0.010
RDE	$\sigma(\Omega_m)$	0.040	0.024
	$\sigma(h)$	–	0.023
	$\sigma(\gamma)$	0.076	0.0089
	$10^2\sigma(\Omega_b h^2)$	0.54	0.0080

Table 3. Absolute errors (1σ) of the cosmological parameters in the HDE and RDE models by using the FRB3 and CMB+FRB3 data. Here, FRB3 denotes the FRB data with the DM_{host} uncertainty $\sigma_{\text{host}} = 150 \text{ pc cm}^{-3}$.

From table 3, we see that the constraints from FRB3 are slightly looser than those from FRB2. Taking the HDE model as an example, we can see that FRB3 and CMB+FRB3 give the results $\varepsilon(c) = 37.3\%$ and $\varepsilon(c) = 6.7\%$, respectively, which are 2.8% and 6.0% larger than those from FRB2 and CMB+FRB2, respectively. The influence on the constraints in the RDE model is slightly larger. The relative errors in the cases of FRB3 and CMB+FRB3 are $\varepsilon(\gamma) = 27.9\%$ and $\varepsilon(\gamma) = 3.8\%$, which are 20.4% and 8.7% larger than those from FRB2 and CMB+FRB2, respectively. From eq. (2.18), we see that σ_{host} contributes to the total uncertainty of DM_{IGM} with a factor $1/(1+z)$, thus even though σ_{host} varies a lot, its impact on FRBs’ capability of constraining cosmological parameters and breaking parameter degeneracies is slight. So, there may be some other factors affecting the constraints, but the main conclusions will still hold. This confirms the discussion in ref. [61].

4 Conclusion

In this paper, we investigate the capability of future FRB data in improving the cosmological parameter estimation and how many FRB data are required to effectively constrain the cosmological parameters in the HDE and RDE models. We consider two FRB scenarios: the normal expectation scenario with 1000 localized FRB data and the optimistic expectation scenario with 10000 localized FRB data.

We find that, in the HDE model, combining the FRB data and the CMB data could break the parameter degeneracies, and the joint constraints on H_0 and dark-energy parameters are quite tight. To achieve the constraint precision of H_0 comparable with the SH0ES result [142], around 10000 FRB data are need to be combined with the CMB data. For the EoS of dark energy, 10000 FRB data combined with the CMB data would give a $\sim 6\%$ constraint, which is close to the precision given by the CMB+BAO+SN data. The data combination FRB+CMB also give a tight constraint on $\Omega_b h^2$. The results in the RDE model also support the conclusion above. These results confirm the conclusion in ref. [61] that the future 10^4 FRB data can become useful in cosmological parameter estimation when combined with CMB.

We also consider another powerful low-redshift cosmological probe, the GW standard sirens observation, and investigate the capability of constraining cosmological parameters when combining the FRB data with the GW data, which is independent of CMB. We use a full Fisher matrix analysis to account for the parameter correlations and avoid biased results. The inclusion of the FRB data in the data combination GW+FRB only improves the constraints slightly, but we show that the orientations of the parameter degeneracies formed by FRB and by GW are nearly orthogonal. We show that in some dark energy models such as the HDE model, 10000 FRB events are possibly not enough to be used to constrain cosmological parameters when combined with the GW data. However, we can expect that, in the near future, large amounts of localized FRBs will be observed by SKA. If we could observe much more FRBs with higher precision in the future, the combination with the GW data could significantly improve the constraints. It can be expected that FRBs observed by SKA may have potential to help the joint constraint on c achieve the precision around 1%, reaching the standard of precision cosmology.

Finally, we investigate the effect of the DM_{host} uncertainty on the constraint results. A larger DM_{host} uncertainty surely loses the constraints, but the main conclusions still hold.

Acknowledgments

We thank Zheng-Xiang Li, He Gao, Jing-Zhao Qi, Shang-Jie Jin, Li-Yang Gao, Peng-Ju Wu, Hai-Li Li, Yi-Chao Li, and Di Li for helpful discussions. This work was supported by the National Natural Science Foundation of China (Grants Nos. 11975072, 11835009, 11875102, and 11690021), the Liaoning Revitalization Talents Program (Grant No. XLYC1905011), the Fundamental Research Funds for the Central Universities (Grant No. N2005030), the National Program for Support of Top-Notch Young Professionals (Grant No. W02070050), the Science Research Grants from the China Manned Space Project (Grant No. CMS-CSST-2021-B01), and the National 111 Project of China (Grant No. B16009).

References

- [1] SUPERNOVA SEARCH TEAM collaboration, *Observational evidence from supernovae for an accelerating universe and a cosmological constant*, *Astron. J.* **116** (1998) 1009 [[astro-ph/9805201](#)].
- [2] SUPERNOVA COSMOLOGY PROJECT collaboration, *Measurements of Ω and Λ from 42 high redshift supernovae*, *Astrophys. J.* **517** (1999) 565 [[astro-ph/9812133](#)].
- [3] PLANCK collaboration, *Planck 2018 results. VI. Cosmological parameters*, *Astron. Astrophys.* **641** (2020) A6 [[1807.06209](#)].
- [4] N.A. Bahcall, J.P. Ostriker, S. Perlmutter and P.J. Steinhardt, *The Cosmic triangle: Assessing the state of the universe*, *Science* **284** (1999) 1481 [[astro-ph/9906463](#)].
- [5] S. Weinberg, *The Cosmological Constant Problem*, *Rev. Mod. Phys.* **61** (1989) 1.
- [6] A. Joyce, B. Jain, J. Khoury and M. Trodden, *Beyond the Cosmological Standard Model*, *Phys. Rept.* **568** (2015) 1 [[1407.0059](#)].
- [7] M. Zhao, R. Guo, D. He, J. Zhang and X. Zhang, *Dark energy versus modified gravity: Impacts on measuring neutrino mass*, *Sci. China Phys. Mech. Astron.* **63** (2020) 230412 [[1810.11658](#)].

- [8] L. Feng, H.-L. Li, J.-F. Zhang and X. Zhang, *Exploring neutrino mass and mass hierarchy in interacting dark energy models*, *Sci. China Phys. Mech. Astron.* **63** (2020) 220401 [1903.08848].
- [9] H.-L. Li, L. Feng, J.-F. Zhang and X. Zhang, *Models of vacuum energy interacting with cold dark matter: Constraints and comparison*, *Sci. China Phys. Mech. Astron.* **62** (2019) 120411 [1812.00319].
- [10] PLANCK collaboration, *Planck 2018 results. I. Overview and the cosmological legacy of Planck*, *Astron. Astrophys.* **641** (2020) A1 [1807.06205].
- [11] F. Beutler, C. Blake, M. Colless, D.H. Jones, L. Staveley-Smith, L. Campbell et al., *The 6dF Galaxy Survey: Baryon Acoustic Oscillations and the Local Hubble Constant*, *Mon. Not. Roy. Astron. Soc.* **416** (2011) 3017 [1106.3366].
- [12] A.J. Ross, L. Samushia, C. Howlett, W.J. Percival, A. Burden and M. Manera, *The clustering of the SDSS DR7 main Galaxy sample – I. A 4 per cent distance measure at $z = 0.15$* , *Mon. Not. Roy. Astron. Soc.* **449** (2015) 835 [1409.3242].
- [13] BOSS collaboration, *The clustering of galaxies in the completed SDSS-III Baryon Oscillation Spectroscopic Survey: cosmological analysis of the DR12 galaxy sample*, *Mon. Not. Roy. Astron. Soc.* **470** (2017) 2617 [1607.03155].
- [14] D.R. Lorimer, M. Bailes, M.A. McLaughlin, D.J. Narkevic and F. Crawford, *A bright millisecond radio burst of extragalactic origin*, *Science* **318** (2007) 777 [0709.4301].
- [15] E.F. Keane, B.W. Stappers, M. Kramer and A.G. Lyne, *On the origin of a highly-dispersed coherent radio burst*, *Mon. Not. Roy. Astron. Soc.* **425** (2012) 71 [1206.4135].
- [16] D. Thornton et al., *A Population of Fast Radio Bursts at Cosmological Distances*, *Science* **341** (2013) 53 [1307.1628].
- [17] CHIME/FRB collaboration, *The First CHIME/FRB Fast Radio Burst Catalog*, 2106.04352.
- [18] L.G. Spitler et al., *A Repeating Fast Radio Burst*, *Nature* **531** (2016) 202 [1603.00581].
- [19] S. Chatterjee et al., *The direct localization of a fast radio burst and its host*, *Nature* **541** (2017) 58 [1701.01098].
- [20] S.P. Tendulkar et al., *The Host Galaxy and Redshift of the Repeating Fast Radio Burst FRB 121102*, *Astrophys. J. Lett.* **834** (2017) L7 [1701.01100].
- [21] M. Kokubo et al., *H α intensity map of the repeating fast radio burst FRB 121102 host galaxy from Subaru/Kyoto 3DII AO-assisted optical integral-field spectroscopy*, *Astrophys. J.* **844** (2017) 95 [1705.04693].
- [22] C.G. Bassa et al., *FRB 121102 is coincident with a star forming region in its host galaxy*, *Astrophys. J. Lett.* **843** (2017) L8 [1705.07698].
- [23] J.X. Prochaska, J.-P. Macquart, M. McQuinn, S. Simha, R.M. Shannon, C.K. Day et al., *The low density and magnetization of a massive galaxy halo exposed by a fast radio burst*, *Science* **366** (2019) 231 [<https://science.sciencemag.org/content/366/6462/231.full.pdf>].
- [24] V. Ravi et al., *A fast radio burst localized to a massive galaxy*, *Nature* **572** (2019) 352 [1907.01542].
- [25] K.W. Bannister et al., *A single fast radio burst localized to a massive galaxy at cosmological distance*, 1906.11476.
- [26] CHIME/FRB collaboration, *Periodic activity from a fast radio burst source*, 2001.10275.
- [27] J.S. Chittidi, S. Simha, A. Mannings, J.X. Prochaska, M. Rafelski, M. Neeleman et al., *Dissecting the local environment of frb 190608 in the spiral arm of its host galaxy*, *arXiv preprint arXiv:2005.13158* (2020) .

- [28] S. Bhandari et al., *The host galaxies and progenitors of Fast Radio Bursts localized with the Australian Square Kilometre Array Pathfinder*, *Astrophys. J. Lett.* **895** (2020) L37 [2005.13160].
- [29] A.G. Mannings, W.-f. Fong, S. Simha, J.X. Prochaska, M. Rafelski, C.D. Kilpatrick et al., *A high-resolution view of fast radio burst host environments*, *arXiv preprint arXiv:2012.11617* (2020) .
- [30] B. Marcote et al., *A repeating fast radio burst source localized to a nearby spiral galaxy*, *Nature* **577** (2020) 190 [2001.02222].
- [31] J.P. Macquart et al., *A census of baryons in the Universe from localized fast radio bursts*, *Nature* **581** (2020) 391 [2005.13161].
- [32] C.W. James, J.X. Prochaska, J.P. Macquart, F. North-Hickey, K.W. Bannister and A. Dunning, *The fast radio burst population evolves with the star-formation rate*, [2101.07998](#).
- [33] M. Bhardwaj et al., *A Nearby Repeating Fast Radio Burst in the Direction of M81*, *Astrophys. J. Lett.* **910** (2021) L18 [2103.01295].
- [34] C.J. Law et al., *A Distant Fast Radio Burst Associated with Its Host Galaxy by the Very Large Array*, *Astrophys. J.* **899** (2020) 161 [2007.02155].
- [35] K.E. Heintz, J.X. Prochaska, S. Simha, E. Platts, W.-f. Fong, N. Tejos et al., *Host galaxy properties and offset distributions of fast radio bursts: implications for their progenitors*, *The Astrophysical Journal* **903** (2020) 152.
- [36] S. Simha, J.N. Burchett, J.X. Prochaska, J.S. Chittidi, O. Elek, N. Tejos et al., *Disentangling the cosmic web toward frb 190608*, *The Astrophysical Journal* **901** (2020) 134.
- [37] W. Deng and B. Zhang, *Cosmological Implications of Fast Radio Burst/Gamma-Ray Burst Associations*, *Astrophys. J. Lett.* **783** (2014) L35 [1401.0059].
- [38] H. Gao, Z. Li and B. Zhang, *Fast Radio Burst/Gamma-Ray Burst Cosmography*, *Astrophys. J.* **788** (2014) 189 [1402.2498].
- [39] Q. Wu, H. Yu and F.Y. Wang, *A New Method to Measure Hubble Parameter $H(z)$ using Fast Radio Bursts*, *Astrophys. J.* **895** (2020) 33 [2004.12649].
- [40] S. Hagstotz, R. Reischke and R. Lilow, *A new measurement of the Hubble constant using Fast Radio Bursts*, [2104.04538](#).
- [41] Q. Wu, G.Q. Zhang and F.Y. Wang, *An 8% Determination of the Hubble Constant from localized Fast Radio Bursts*, [2108.00581](#).
- [42] B. Zhou, X. Li, T. Wang, Y.-Z. Fan and D.-M. Wei, *Fast radio bursts as a cosmic probe?*, *Phys. Rev. D* **89** (2014) 107303 [1401.2927].
- [43] M. Jaroszynski, *Fast Radio Bursts and cosmological tests*, *Mon. Not. Roy. Astron. Soc.* **484** (2019) 1637 [1812.11936].
- [44] A. Walters, Y.-Z. Ma, J. Sievers and A. Weltman, *Probing Diffuse Gas with Fast Radio Bursts*, *Phys. Rev. D* **100** (2019) 103519 [1909.02821].
- [45] K.-G. Lee, M. Ata, I.S. Khrykin, Y. Huang, J.X. Prochaska, J. Cooke et al., *Constraining the Cosmic Baryon Distribution with Fast Radio Burst Foreground Mapping*, [2109.00386](#).
- [46] E.V. Linder, *Detecting Helium Reionization with Fast Radio Bursts*, *Phys. Rev. D* **101** (2020) 103019 [2001.11517].
- [47] P. Kumar and E.V. Linder, *On the Use of Fast Radio Burst Dispersion Measures as Distance Measures*, *Phys. Rev. D* **100** (2019) 083533 [1903.08175].
- [48] J.B. Muñoz, E.D. Kovetz, L. Dai and M. Kamionkowski, *Lensing of Fast Radio Bursts as a Probe of Compact Dark Matter*, *Phys. Rev. Lett.* **117** (2016) 091301 [1605.00008].

- [49] Y.K. Wang and F.Y. Wang, *Lensing of Fast Radio Bursts by Binaries to Probe Compact Dark Matter*, *Astron. Astrophys.* **614** (2018) A50 [[1801.07360](#)].
- [50] J.-J. Wei, H. Gao, X.-F. Wu and P. Mészáros, *Testing Einstein’s Equivalence Principle With Fast Radio Bursts*, *Phys. Rev. Lett.* **115** (2015) 261101 [[1512.07670](#)].
- [51] H. Yu and F.Y. Wang, *Testing Weak Equivalence Principle with Strongly Lensed Cosmic Transients*, *Eur. Phys. J. C* **78** (2018) 692 [[1801.01257](#)].
- [52] N. Xing, H. Gao, J. Wei, Z. Li, W. Wang, B. Zhang et al., *Limits on the Weak Equivalence Principle and Photon Mass with FRB 121102 Subpulses*, *Astrophys. J. Lett.* **882** (2019) L13 [[1907.00583](#)].
- [53] Y.-P. Yang and B. Zhang, *Extracting host galaxy dispersion measure and constraining cosmological parameters using fast radio burst data*, *Astrophys. J. Lett.* **830** (2016) L31 [[1608.08154](#)].
- [54] Z.-X. Li, H. Gao, X.-H. Ding, G.-J. Wang and B. Zhang, *Strongly lensed repeating fast radio bursts as precision probes of the universe*, *Nature Commun.* **9** (2018) 3833 [[1708.06357](#)].
- [55] B. Liu, Z. Li, H. Gao and Z.-H. Zhu, *Prospects of strongly lensed repeating fast radio bursts: Complementary constraints on dark energy evolution*, *Phys. Rev. D* **99** (2019) 123517 [[1907.10488](#)].
- [56] H. Yu and F.Y. Wang, *Measuring the cosmic proper distance from fast radio bursts*, *Astron. Astrophys.* **606** (2017) A3 [[1708.06905](#)].
- [57] A. Walters, A. Weltman, B.M. Gaensler, Y.-Z. Ma and A. Witzemann, *Future Cosmological Constraints from Fast Radio Bursts*, *Astrophys. J.* **856** (2018) 65 [[1711.11277](#)].
- [58] S. Bhandari and C. Flynn, *Probing the Universe with Fast Radio Bursts*, *Universe* **7** (2021) 85.
- [59] J.-J. Wei, X.-F. Wu and H. Gao, *Cosmology with Gravitational Wave/Fast Radio Burst Associations*, *Astrophys. J. Lett.* **860** (2018) L7 [[1805.12265](#)].
- [60] Z. Li, H. Gao, J.-J. Wei, Y.-P. Yang, B. Zhang and Z.-H. Zhu, *Cosmology-independent estimate of the fraction of baryon mass in the IGM from fast radio burst observations*, *Astrophys. J.* **876** (2019) 146 [[1904.08927](#)].
- [61] Z.-W. Zhao, Z.-X. Li, J.-Z. Qi, H. Gao, J.-F. Zhang and X. Zhang, *Cosmological parameter estimation for dynamical dark energy models with future fast radio burst observations*, *Astrophys. J.* **903** (2020) 83 [[2006.01450](#)].
- [62] B.F. Schutz, *Determining the Hubble Constant from Gravitational Wave Observations*, *Nature* **323** (1986) 310.
- [63] D.E. Holz and S.A. Hughes, *Using gravitational-wave standard sirens*, *Astrophys. J.* **629** (2005) 15 [[astro-ph/0504616](#)].
- [64] W. Zhao, C. Van Den Broeck, D. Baskaran and T.G.F. Li, *Determination of Dark Energy by the Einstein Telescope: Comparing with CMB, BAO and SNIa Observations*, *Phys. Rev. D* **83** (2011) 023005 [[1009.0206](#)].
- [65] J.-F. Zhang, M. Zhang, S.-J. Jin, J.-Z. Qi and X. Zhang, *Cosmological parameter estimation with future gravitational wave standard siren observation from the Einstein Telescope*, *JCAP* **09** (2019) 068 [[1907.03238](#)].
- [66] X.-N. Zhang, L.-F. Wang, J.-F. Zhang and X. Zhang, *Improving cosmological parameter estimation with the future gravitational-wave standard siren observation from the Einstein Telescope*, *Phys. Rev. D* **99** (2019) 063510 [[1804.08379](#)].
- [67] X. Zhang, *Gravitational wave standard sirens and cosmological parameter measurement*, *Sci. China Phys. Mech. Astron.* **62** (2019) 110431 [[1905.11122](#)].

- [68] H.-L. Li, D.-Z. He, J.-F. Zhang and X. Zhang, *Quantifying the impacts of future gravitational-wave data on constraining interacting dark energy*, *JCAP* **06** (2020) 038 [[1908.03098](#)].
- [69] R.-G. Cai, T.-B. Liu, X.-W. Liu, S.-J. Wang and T. Yang, *Probing cosmic anisotropy with gravitational waves as standard sirens*, *Phys. Rev. D* **97** (2018) 103005 [[1712.00952](#)].
- [70] R.-G. Cai and T. Yang, *Estimating cosmological parameters by the simulated data of gravitational waves from the Einstein Telescope*, *Phys. Rev. D* **95** (2017) 044024 [[1608.08008](#)].
- [71] KAGRA, LIGO SCIENTIFIC, VIRGO collaboration, *Prospects for Observing and Localizing Gravitational-Wave Transients with Advanced LIGO, Advanced Virgo and KAGRA*, *Living Rev. Rel.* **21** (2018) 3 [[1304.0670](#)].
- [72] L.-F. Wang, X.-N. Zhang, J.-F. Zhang and X. Zhang, *Impacts of gravitational-wave standard siren observation of the Einstein Telescope on weighing neutrinos in cosmology*, *Phys. Lett. B* **782** (2018) 87 [[1802.04720](#)].
- [73] L.-F. Wang, Z.-W. Zhao, J.-F. Zhang and X. Zhang, *A preliminary forecast for cosmological parameter estimation with gravitational-wave standard sirens from TianQin*, *JCAP* **11** (2020) 012 [[1907.01838](#)].
- [74] L.-F. Wang, S.-J. Jin, J.-F. Zhang and X. Zhang, *Forecast for cosmological parameter estimation with gravitational-wave standard sirens from the LISA-Taiji network*, [2101.11882](#).
- [75] S.-J. Jin, D.-Z. He, Y. Xu, J.-F. Zhang and X. Zhang, *Forecast for cosmological parameter estimation with gravitational-wave standard siren observation from the Cosmic Explorer*, *JCAP* **03** (2020) 051 [[2001.05393](#)].
- [76] S.-J. Jin, L.-F. Wang, P.-J. Wu, J.-F. Zhang and X. Zhang, *How can gravitational-wave standard sirens and 21 cm intensity mapping jointly provide a precise late-universe cosmological probe?*, [2106.01859](#).
- [77] Z.-W. Zhao, L.-F. Wang, J.-F. Zhang and X. Zhang, *Prospects for improving cosmological parameter estimation with gravitational-wave standard sirens from Taiji*, *Sci. Bull.* **65** (2020) 1340 [[1912.11629](#)].
- [78] M. Li, *A Model of holographic dark energy*, *Phys. Lett. B* **603** (2004) 1 [[hep-th/0403127](#)].
- [79] S. Wang, Y. Wang and M. Li, *Holographic Dark Energy*, *Phys. Rept.* **696** (2017) 1 [[1612.00345](#)].
- [80] C. Lin, *An effective field theory of holographic dark energy*, [2101.08092](#).
- [81] A. Ganz and C. Lin, *Structure Formation in the Effective Field Theory of Holographic Dark Energy*, [2109.07420](#).
- [82] X. Zhang and F.-Q. Wu, *Constraints on holographic dark energy from Type Ia supernova observations*, *Phys. Rev. D* **72** (2005) 043524 [[astro-ph/0506310](#)].
- [83] X. Zhang and F.-Q. Wu, *Constraints on Holographic Dark Energy from Latest Supernovae, Galaxy Clustering, and Cosmic Microwave Background Anisotropy Observations*, *Phys. Rev. D* **76** (2007) 023502 [[astro-ph/0701405](#)].
- [84] Z. Chang, F.-Q. Wu and X. Zhang, *Constraints on holographic dark energy from x-ray gas mass fraction of galaxy clusters*, *Phys. Lett. B* **633** (2006) 14 [[astro-ph/0509531](#)].
- [85] M. Li, X.-D. Li, Y.-Z. Ma, X. Zhang and Z. Zhang, *Planck Constraints on Holographic Dark Energy*, *JCAP* **09** (2013) 021 [[1305.5302](#)].
- [86] Y.-Y. Xu and X. Zhang, *Comparison of dark energy models after Planck 2015*, *Eur. Phys. J. C* **76** (2016) 588 [[1607.06262](#)].
- [87] Q.-G. Huang and Y.-G. Gong, *Supernova constraints on a holographic dark energy model*, *JCAP* **08** (2004) 006 [[astro-ph/0403590](#)].

- [88] C. Feng, B. Wang, Y. Gong and R.-K. Su, *Testing the viability of the interacting holographic dark energy model by using combined observational constraints*, *JCAP* **09** (2007) 005 [0706.4033].
- [89] Y.-Z. Ma, Y. Gong and X. Chen, *Features of holographic dark energy under the combined cosmological constraints*, *Eur. Phys. J. C* **60** (2009) 303 [0711.1641].
- [90] I.A. Akhlaghi, M. Malekjani, S. Basilakos and H. Haghi, *Model selection and constraints from Holographic dark energy scenarios*, *Mon. Not. Roy. Astron. Soc.* **477** (2018) 3659 [1804.02989].
- [91] E. Sadri and M. Khurshudyan, *An interacting new holographic dark energy model: Observational constraints*, *Int. J. Mod. Phys. D* **28** (2019) 1950152 [1809.07595].
- [92] W.-M. Dai, Y.-Z. Ma and H.-J. He, *Reconciling Hubble Constant Discrepancy from Holographic Dark Energy*, *Phys. Rev. D* **102** (2020) 121302 [2003.03602].
- [93] C. Gao, F. Wu, X. Chen and Y.-G. Shen, *A Holographic Dark Energy Model from Ricci Scalar Curvature*, *Phys. Rev. D* **79** (2009) 043511 [0712.1394].
- [94] X. Zhang, *Holographic Ricci dark energy: Current observational constraints, quintom feature, and the reconstruction of scalar-field dark energy*, *Phys. Rev. D* **79** (2009) 103509 [0901.2262].
- [95] A.G. Cohen, D.B. Kaplan and A.E. Nelson, *Effective field theory, black holes, and the cosmological constant*, *Phys. Rev. Lett.* **82** (1999) 4971 [hep-th/9803132].
- [96] S.D.H. Hsu, *Entropy bounds and dark energy*, *Phys. Lett. B* **594** (2004) 13 [hep-th/0403052].
- [97] A.M. Hopkins and J.F. Beacom, *On the normalisation of the cosmic star formation history*, *Astrophys. J.* **651** (2006) 142 [astro-ph/0601463].
- [98] M. Caleb, C. Flynn, M. Bailes, E.D. Barr, R.W. Hunstead, E.F. Keane et al., *Are the distributions of Fast Radio Burst properties consistent with a cosmological population?*, *Mon. Not. Roy. Astron. Soc.* **458** (2016) 708 [1512.02738].
- [99] 2dFGRS collaboration, *The 2dF Galaxy Redshift Survey: Near infrared galaxy luminosity functions*, *Mon. Not. Roy. Astron. Soc.* **326** (2001) 255 [astro-ph/0012429].
- [100] J.M. Shull, B.D. Smith and C.W. Danforth, *The Baryon Census in a Multiphase Intergalactic Medium: 30% of the Baryons May Still Be Missing*, *Astrophys. J.* **759** (2012) 23 [1112.2706].
- [101] X.-H. Fan, C.L. Carilli and B.G. Keating, *Observational constraints on cosmic reionization*, *Ann. Rev. Astron. Astrophys.* **44** (2006) 415 [astro-ph/0602375].
- [102] E. Petroff, E.D. Barr, A. Jameson, E.F. Keane, M. Bailes, M. Kramer et al., *FRBCAT: The Fast Radio Burst Catalogue*, *Publ. Astron. Soc. Austral.* **33** (2016) e045 [1601.03547].
- [103] R.N. Manchester, G.B. Hobbs, A. Teoh and M. Hobbs, *The Australia Telescope National Facility pulsar catalogue*, *Astron. J.* **129** (2005) 1993 [astro-ph/0412641].
- [104] T. Hashimoto, T. Goto, A.Y.L. On, T.-Y. Lu, D.J.D. Santos, S.C.C. Ho et al., *Fast radio bursts to be detected with the Square Kilometre Array*, *Mon. Not. Roy. Astron. Soc.* **497** (2020) 4107 [2008.00007].
- [105] C.A. Faucher-Giguere, D. Keres and C.P. Ma, *The Baryonic Assembly of Dark Matter Halos*, *Mon. Not. Roy. Astron. Soc.* **417** (2011) 2982 [1103.0001].
- [106] M. McQuinn, *Locating the "missing" baryons with extragalactic dispersion measure estimates*, *Astrophys. J. Lett.* **780** (2014) L33 [1309.4451].
- [107] L. Connor, H.-H. Lin, K. Masui, N. Oppermann, U.-L. Pen, J.B. Peterson et al., *Constraints on the FRB rate at 700–900 MHz*, *Mon. Not. Roy. Astron. Soc.* **460** (2016) 1054 [1602.07292].

- [108] J.-P. Macquart and R. Ekers, *FRB event rate counts – II. Fluence, redshift, and dispersion measure distributions*, *Mon. Not. Roy. Astron. Soc.* **480** (2018) 4211 [1808.00908].
- [109] R. Luo, Y. Men, K. Lee, W. Wang, D.R. Lorimer and B. Zhang, *On the FRB luminosity function – II. Event rate density*, *Mon. Not. Roy. Astron. Soc.* **494** (2020) 665 [2003.04848].
- [110] D. Lorimer, *CHIME rings in its first catalogue*, *Nature Astron.* **5** (2021) 870.
- [111] G. Hallinan et al., *The DSA-2000 – A Radio Survey Camera*, 1907.07648.
- [112] L.B. Newburgh et al., *HIRAX: A Probe of Dark Energy and Radio Transients*, *Proc. SPIE Int. Soc. Opt. Eng.* **9906** (2016) 99065X [1607.02059].
- [113] R. Schneider, V. Ferrari, S. Matarrese and S.F. Portegies Zwart, *Gravitational waves from cosmological compact binaries*, *Mon. Not. Roy. Astron. Soc.* **324** (2001) 797 [astro-ph/0002055].
- [114] C. Cutler and D.E. Holz, *Ultra-high precision cosmology from gravitational waves*, *Phys. Rev. D* **80** (2009) 104009 [0906.3752].
- [115] B.S. Sathyaprakash and B.F. Schutz, *Physics, Astrophysics and Cosmology with Gravitational Waves*, *Living Rev. Rel.* **12** (2009) 2 [0903.0338].
- [116] L. Blanchet and B.R. Iyer, *Hadamard regularization of the third post-Newtonian gravitational wave generation of two point masses*, *Phys. Rev. D* **71** (2005) 024004 [gr-qc/0409094].
- [117] <https://www.et-gw.eu/index.php/etsensitivities/>.
- [118] T.G. Li, *Extracting physics from gravitational waves: testing the strong-field dynamics of general relativity and inferring the large-scale structure of the Universe*, Springer (2015).
- [119] C.M. Hirata, D.E. Holz and C. Cutler, *Reducing the weak lensing noise for the gravitational wave Hubble diagram using the non-Gaussianity of the magnification distribution*, *Phys. Rev. D* **81** (2010) 124046 [1004.3988].
- [120] N. Tamanini, C. Caprini, E. Barausse, A. Sesana, A. Klein and A. Petiteau, *Science with the space-based interferometer eLISA. III: Probing the expansion of the Universe using gravitational wave standard sirens*, *JCAP* **04** (2016) 002 [1601.07112].
- [121] L. Speri, N. Tamanini, R.R. Caldwell, J.R. Gair and B. Wang, *Testing the Quasar Hubble Diagram with LISA Standard Sirens*, *Phys. Rev. D* **103** (2021) 083526 [2010.09049].
- [122] T. Yang, *Gravitational-Wave Detector Networks: Standard Sirens on Cosmology and Modified Gravity Theory*, *JCAP* **05** (2021) 044 [2103.01923].
- [123] B. Kocsis, Z. Frei, Z. Haiman and K. Menou, *Finding the electromagnetic counterparts of cosmological standard sirens*, *Astrophys. J.* **637** (2006) 27 [astro-ph/0505394].
- [124] P.A. Evans et al., *Swift and NuSTAR observations of GW170817: detection of a blue kilonova*, *Science* **358** (2017) 1565 [1710.05437].
- [125] J. Yu, H. Song, S. Ai, H. Gao, F. Wang, Y. Wang et al., *Multi-messenger Detection Rates and distributions of Binary Neutron Star Mergers and Their Cosmological Implications*, 2104.12374.
- [126] H.-Y. Chen, P.S. Cowperthwaite, B.D. Metzger and E. Berger, *A Program for Multimessenger Standard Siren Cosmology in the Era of LIGO A+, Rubin Observatory, and Beyond*, *Astrophys. J. Lett.* **908** (2021) L4 [2011.01211].
- [127] L. Chen, Q.-G. Huang and K. Wang, *Distance Priors from Planck Final Release*, *JCAP* **02** (2019) 028 [1808.05724].
- [128] J.-F. Zhang, H.-Y. Dong, J.-Z. Qi and X. Zhang, *Prospect for constraining holographic dark energy with gravitational wave standard sirens from the Einstein Telescope*, *Eur. Phys. J. C* **80** (2020) 217 [1906.07504].

- [129] A. Lewis and S. Bridle, *Cosmological parameters from CMB and other data: A Monte Carlo approach*, *Phys. Rev. D* **66** (2002) 103511 [[astro-ph/0205436](#)].
- [130] S. Driver, *The challenge of measuring and mapping the missing baryons*, *Nature Astronomy* (2021) 1.
- [131] A.G. Riess, *The Expansion of the Universe is Faster than Expected*, *Nature Rev. Phys.* **2** (2019) 10 [[2001.03624](#)].
- [132] L. Verde, T. Treu and A.G. Riess, *Tensions between the Early and the Late Universe*, *Nature Astron.* **3** (2019) 891 [[1907.10625](#)].
- [133] R.-Y. Guo, J.-F. Zhang and X. Zhang, *Can the H_0 tension be resolved in extensions to Λ CDM cosmology?*, *JCAP* **02** (2019) 054 [[1809.02340](#)].
- [134] R.-G. Cai, *Editorial*, *Sci. China Phys. Mech. Astron.* **63** (2020) 290401.
- [135] M. Liu, Z. Huang, X. Luo, H. Miao, N.K. Singh and L. Huang, *Can Non-standard Recombination Resolve the Hubble Tension?*, *Sci. China Phys. Mech. Astron.* **63** (2020) 290405 [[1912.00190](#)].
- [136] X. Zhang and Q.-G. Huang, *Measuring H_0 from low- z datasets*, *Sci. China Phys. Mech. Astron.* **63** (2020) 290402 [[1911.09439](#)].
- [137] Q. Ding, T. Nakama and Y. Wang, *A gigaparsec-scale local void and the Hubble tension*, *Sci. China Phys. Mech. Astron.* **63** (2020) 290403 [[1912.12600](#)].
- [138] R.-Y. Guo, J.-F. Zhang and X. Zhang, *Inflation model selection revisited after a 1.91% measurement of the Hubble constant*, *Sci. China Phys. Mech. Astron.* **63** (2020) 290406 [[1910.13944](#)].
- [139] R.-Y. Guo, L. Zhang, J.-F. Zhang and X. Zhang, *Constraints on brane inflation after Planck 2015: Impacts of the latest local measurement of the Hubble constant*, *Sci. China Phys. Mech. Astron.* **62** (2019) 30411 [[1801.02187](#)].
- [140] L. Feng, D.-Z. He, H.-L. Li, J.-F. Zhang and X. Zhang, *Constraints on active and sterile neutrinos in an interacting dark energy cosmology*, *Sci. China Phys. Mech. Astron.* **63** (2020) 290404 [[1910.03872](#)].
- [141] L.-Y. Gao, Z.-W. Zhao, S.-S. Xue and X. Zhang, *Relieving the H_0 tension with a new interacting dark energy model*, *JCAP* **07** (2021) 005 [[2101.10714](#)].
- [142] A.G. Riess, S. Casertano, W. Yuan, L.M. Macri and D. Scolnic, *Large Magellanic Cloud Cepheid Standards Provide a 1% Foundation for the Determination of the Hubble Constant and Stronger Evidence for Physics beyond Λ CDM*, *Astrophys. J.* **876** (2019) 85 [[1903.07603](#)].